Chirped-pulse control of carriers in semiconductors: the role of many-body effects

Boris D. Fainberg

Department of Sciences, Holon Academic Institute of Technology, 52 Golomb St., Holon 58102, Israel and Raymond and Beverly Sackler Faculty of Exact Sciences, School of Chemistry, Tel-Aviv University, Tel-Aviv 69978, Israel

B. Levinsky and V. A. Gorbunov

Department of Sciences, Holon Academic Institute of Technology, 52 Golomb St., Holon 58102, Israel

Received March 1, 2005; revised manuscript received July 7, 2005; accepted July 20, 2005

The possibility of realizing adiabatic rapid passage (ARP) with an intense chirped-pulse excitation (a concept well known in molecular systems) in direct-gap semiconductors is studied. Based on the semiconductor Bloch equations, the analysis shows that, in spite of complications due to band structure, signatures of ARP accompanied by an intrapulse pump-dump process (IPDP) should be observable in the dependence of the carriers' density on the chirp rate in the frequency domain. The bandgap shrinkage, which is the main many-body effect, gives the dominant contribution to the asymmetry of this dependence on the chirp sign. We show that the bandgap shrinkage enlarges the carriers' density and makes a major impact on the interplay of ARP with IPDP, enhancing ARP (suppressing IPDP) for positive chirped-pulse excitation and suppressing ARP (enhancing IPDP) for negative chirped-pulse excitation.

OCIS codes: 320.1590, 320.7130.

1. INTRODUCTION

Selective population transfer with phase-modulated (chirped) pulses has applications in a number of areas, such as the preparation of initial states for spectroscopy,[1] optical quantum control of atoms, molecules,[2–6] and semiconductors[7] (see Ref. 8, devoted to adiabatic population transfer with a pair of delayed nonchirped pulses in quantum wells, as well as Ref. 9) and Bose–Einstein condensates.[10] In this work we concentrate on generating carriers in bulk direct-gap semiconductors, which are interesting for their use in electro-optical devices. Pulse chirping has the potential to improve and optimize all-optical ultrafast switching.

Chirped pulses are very effective in selective population transfer between molecular electronic states, owing to adiabatic rapid passage (ARP)[1,3,11–14] and the intrapulse pump-dump process (IPDP).[15,16] ARP enables us to transfer the entire population from ground $|1\rangle$ to the excited $|2\rangle$ electronic state. IPDP creates a nonstationary ground-state component.[17]

An ARP is based on a sweeping of the pulse frequency through a resonance. The mechanism of an ARP can be explained by avoiding the crossing of dressed (adiabatic) states

$$\Phi_{\pm}(t) = \begin{bmatrix} \sin \vartheta(t) \\ \cos \vartheta(t) \end{bmatrix} |1\rangle \pm \begin{bmatrix} \cos \vartheta(t) \\ \sin \vartheta(t) \end{bmatrix} |2\rangle \qquad (1)$$

as a function of the instantaneous laser pulse frequency $\omega(t)$.[3] Here, the mixing angle $\vartheta(t)$ is defined (modulo π) as $\vartheta = (1/2) \arctan [U/\delta(t)]$, where U is the Rabi frequency and $\delta(t)$ is the frequency detuning of $\omega(t)$ with respect to the frequency of transition $1 \rightarrow 2$. During the excitation, the mixing angle rotates clockwise from $\vartheta(-\infty) = \pi/2$ to $\vartheta(+\infty) = 0$, and the composition of adiabatic states changes accordingly. In particular, starting from state $|1\rangle$, the system follows the adiabatic (dressed) state $\Phi_+(t)$ adiabatically and eventually ends up in state $|2\rangle$.[6] A scheme based on ARP is robust, since it is insensitive to pulse area and the precise location of the resonance. Therefore it has many uses, including the preparation of entangled states[18] and initial states for Bose–Einstein condensates.[10]

In the wave-packet picture, IPDP can be explained as follows. The first field interaction places amplitude on the S_1 excited state (pump) (Fig. 1). This amplitude starts to slide down the potential energy surface. A second field interaction can either bring more amplitude up, creating a population in the excited state, or bring the amplitude from the first field interaction back down to S_0, creating a displaced hole in the ground electronic state (dump). Since the wave packet on S_1 is moving from higher optical frequencies to lower, the ground-state population increases for excitation by negatively chirped (NC) pulses. Thus a NC pulse creates a nonstationary ground-state component, whereas a positively chirped (PC) pulse discriminates against it.[16]

ARP in molecules in solution were studied for a two-state electronic system in Refs. 13, 14, and 19 and for a stimulated Raman adiabatic passage configuration in Ref. 20. It was shown in Ref. 13 that relaxation does not hinder coherent population transfer by ARP for PC pulses and moderate detunings of the central pulse frequency

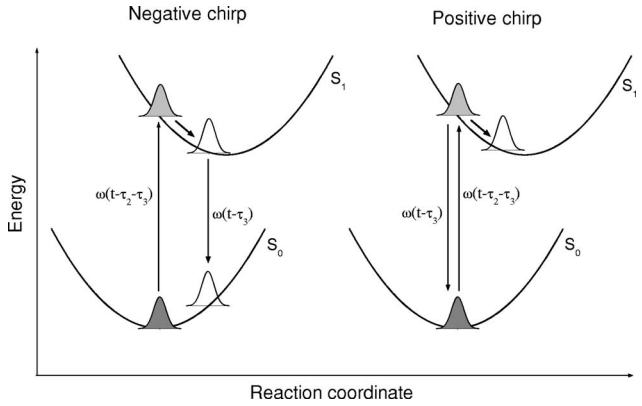

Fig. 1. Diagrams of the intrapulse pump-dump process for NC and PC pulse excitation. The time of the interaction of the excited molecule with light (τ_2) shortens for PC excitation with respect to that for NC excitation. We used designations of the time arguments in accordance with the double-sided Feynman diagrams describing the intrapulse pump-dump process (see Fig. 6 of Ref. 13).

with respect to the frequency of the Franck–Condon transition $1 \rightarrow 2$. Moreover, under these conditions the relaxation favors a more-efficient population transfer with respect to the system with frozen nuclear motion (without relaxation). Such behavior was explained in Ref. 14 by the interplay of ARP with IPDP. The point is that the main adiabatic criterion, $|d\omega(t)/dt| \ll |U|^2$, which is related to the absence of nonadiabatic transitions between dressed states Eq. (1), does not mean a total population transfer between unperturbated states $|1\rangle$ and $|2\rangle$ (also known as the diabatic states). If a transition starts or ends near the avoided crossing where a dressed (adiabatic) state is a superposition of diabatic states, total population transfer does not occur. When the system remains at the avoided crossing, the activation of IPDP is implied. Therefore, to realize total population transfer, in addition to the main adiabatic criterion, a transition must start and end far from resonance (the "second condition to the adiabatic criterion" in terms of Ref. 14); otherwise, only signatures of ARP occur. In particular, a PC pulse excitation is favorable for the fulfillment of the second condition to the adiabatic criterion (see Fig. 1 and the corresponding discussion above).

Optical excitation of direct-gap semiconductors has some similarities to optical transitions in molecules. First, the Franck–Condon principle in molecules is similar to the momentum conservation in direct semiconductors. Second, in the absence of relaxation and the Coulomb carriers' interactions (in semiconductors), the Bloch equations for both the molecular system[13] and the direct-gap semiconductor[21,22] describe an ensemble of independent two-level systems with different transition frequencies corresponding to a pure inhomogeneously broadened optical transition. By this means one would expect the effective control of direct semiconductors using intense chirped pulses from the analogy with molecules.

At the same time, the number of optically generated carriers in a semiconductor is limited by the number of quantum states in the range covered by the spectrum of the exciting pulse (the Pauli exclusion principle). This means that the total population transfer to the conductance band is impossible. Therefore one must keep in mind that the realization of ARP is possible for the quantum transitions only in the excitation region. There are complications owing to band structure in semiconductors as well. Two regions of the avoided crossing of dressed states in momentum space exist and are a limited distance apart. It affects the passage of a system through resonance. In addition, the optical excitation of semiconductors is related to Coulomb electron-hole interactions, the excitation of the partially excited states when the creation of an electron (hole) in the **k** state is not accompanied by creating a hole (electron) in the same state,[23] relaxation times that depend on carriers density, etc. The above processes do not occur in molecular systems.

In the present work, we intend to clarify the following issues: Is it possible to realize an analogy to ARP for direct-gap semiconductors excited with strong chirped pulses? What is the interplay of ARP with IPDP for such systems? What is the role of many-body effects in the excitations under discussion?

Some of the preliminary results in controlling carrier generation in bulk direct-gap semiconductors by intense ultrashort chirped pulses are presented in conference proceedings.[24] Here we give a full account of this study with essentially new results.

The outline of the paper is as follows. In Section 2 we present the Bloch equations for a semiconductor with a direct interband optical transition under the action of chirped pulses. In Subsection 2A we describe approximations for calculating scattering terms, the calculation of which is carried out in Appendices A and B. In Section 3 we solve semiconductor Bloch equations for the total model, which takes into account both the relaxations related to carrier–carrier and carrier–phonon scatterings, and the many-body effects: the bandgap renormalization and Coulomb electron-hole correlations. In Section 4 we formulate a number of approaches to this model. In Section 5 we present the calculation results, analyze the physics that underly the behavior of the approaches to the total model, and compare their behavior with that of the total model. Comparison of the behaviors of different models enables us to study the influence of relaxation and many-body effects on the chirped-pulse control of carriers. In Section 6, by analogy with the time-dependent, light-induced potentials for molecules,[25] we introduce the time-dependent "dressed" states and analyze the time evolution of the weighted nonequilibrium distribution functions. In Subsection 6.1, using the picture of time-dependent renormalized dispersion, we analyze the bandgap renormalization influence on the effective spectral bandwidth of an exciting pulse and the carriers' density value. In Section 7 we summarize our results. In the appendices we present auxiliary calculations.

2. BASIC EQUATIONS

Let us consider a semiconductor with a direct interband optical transition. The semiconductor is affected by a phase-modulated pulse of carrier frequency ω:

$$E(t) = E^{(+)}(t) + E^{(-)}(t) = \frac{1}{2}\mathcal{E}(t)\exp[-i\omega t + i\varphi(t)] + \text{c.c.}, \tag{2}$$

where $\mathcal{E}(t)$ and $\varphi(t)$ are the real functions of time and $\varphi(t)$ describes the change of the pulse phase in time t. The instantaneous pulse frequency is $\omega(t)=\omega-\mathrm{d}\varphi(t)/\mathrm{d}t$.

We describe the ultrafast optical excitation of a semiconductor in the resonance approximation by semiconductor Bloch equations[26,21,23,27] for the distribution functions of electrons, $F^e_{\mathbf{k}}$, and holes, $F^h_{\mathbf{k}}$, and the positive-frequency component of polarization $\mathcal{P}_{\mathbf{k}}(t)=P_{\mathbf{k}}(t)\exp\{-i[\omega t-\varphi(t)]\}$. Switching to the system that rotates with instantaneous frequency $\omega(t)$, $P_{\mathbf{k}}(t)=\mathcal{P}_{\mathbf{k}}(t)\exp\{i[\omega t-\varphi(t)]\}$, we obtain equations for the quantities, which slowly vary with time during the period of a light wave

$$\frac{\mathrm{d}F^c_{\mathbf{k}}}{\mathrm{d}t} = -\,\mathrm{Im}(U_{\mathbf{k}}P^*_{\mathbf{k}}) + \left(\frac{\mathrm{d}F^c_{\mathbf{k}}}{\mathrm{d}t}\right)_{\text{scat}}, \tag{3}$$

$$\frac{\mathrm{d}P_{\mathbf{k}}}{\mathrm{d}t} = i\Delta_{\mathbf{k}}(t)P_{\mathbf{k}} + \frac{i}{2}U_{\mathbf{k}}(1-F^e_{\mathbf{k}}-F^h_{\mathbf{k}}) + \left(\frac{\mathrm{d}P_{\mathbf{k}}}{\mathrm{d}t}\right)_{\text{scat}}, \tag{4}$$

where $c=e,h$;

$$\Delta_{\mathbf{k}}(t) = \omega(t) - \frac{E_g}{\hbar} - \frac{\epsilon_{\mathbf{k}}}{\hbar} = \Delta_0 - \frac{\mathrm{d}\varphi(t)}{\mathrm{d}t} - \frac{\epsilon_{\mathbf{k}}}{\hbar}, \tag{5}$$

where $\Delta_0=\omega-E_g/\hbar$ is the detuning of the carrier pulse frequency ω with respect to the semiconductor optical gap $E_g/\hbar$; $\epsilon_{\mathbf{k}}=\epsilon^0_k+\Delta\epsilon_{\mathbf{k}}$ and $\epsilon^0_k=\epsilon^{0e}_k+\epsilon^{0h}_k=\hbar^2k^2/2m_r$ are the renormalized and kinetic energies, respectively, of an electron-hole pair in a semiconductor with reduced mass $m_r=m_em_h/(m_e+m_h)$; $\epsilon^{0c}_k=\hbar^2k^2/2m_c$ are the kinetic energies of the carriers; $\Delta\epsilon_{\mathbf{k}}=\Delta\epsilon_{\text{CH}}+\Delta\epsilon_{\text{SX},\mathbf{k}}$;

$$\Delta\epsilon_{\text{CH}} = \sum_{\mathbf{q}\neq 0}[V^s(q)-V(q)] \tag{6}$$

is the Debye shift, or the so-called Coulomb-hole self-energy;

$$\Delta\epsilon_{\text{SX},\mathbf{k}} = -\sum_{\mathbf{q}} V^s(q)(F^e_{\mathbf{k}+\mathbf{q}}+F^h_{\mathbf{k}+\mathbf{q}}) \tag{7}$$

is the screened-exchange shift[23]; and

$$U_{\mathbf{k}} = \frac{d_{cv}\mathcal{E}(t)}{\hbar} + \frac{2}{\hbar}\sum_{\mathbf{k}'} V^s(|\mathbf{k}-\mathbf{k}'|)P_{\mathbf{k}'} \tag{8}$$

is the generalized Rabi frequency. Here $V(q)=4\pi e^2/L^3\epsilon_0q^2$ and $V^s(q)$ are unscreened and screened Coulomb potentials, respectively [the formula for $V^s(q)$ is given below]; e is the value of the electron charge, L^3 is the volume; ϵ_0 is the static dielectric constant of the semiconductor; and d_{cv} is the matrix element of the dipole moment. Following Ref. 28, we take into account the dependence of the matrix element of the dipole moment on the carrier energy due to the nonparabolicity of the band structure:

$$d_{cv}(\mathbf{k}) = \frac{d_{cv}}{1+\exp[(\epsilon_{\mathbf{k}}-\epsilon_c)/\hbar\Delta_c]}, \tag{9}$$

where $\epsilon_c=270$ meV and $\hbar\Delta_c=1.05$ meV for bulk GaAs. Such a dependence imposes the limitation on the energy of the carriers' excitation. The quantities $(\mathrm{d}P_{\mathbf{k}}/\mathrm{d}t)_{\text{scat}}$ and $(\mathrm{d}F^c_{\mathbf{k}}/\mathrm{d}t)_{\text{scat}}$ are the carrier–carrier and carrier–phonon scattering terms, respectively. It is worth noting that Eqs. (3), (4), and (6)–(8) are essentially a Hartree–Fock approximation, improved to account for quasi-static screening. Owing to the short exciting pulse duration $t_p\sim 100$ fs, we neglect radiative recombination in Eqs. (3) and (4).

The formulas for quantities $V^s(q)$, $(\mathrm{d}P_{\mathbf{k}}/\mathrm{d}t)_{\text{scat}}$ and $(\mathrm{d}F^c_{\mathbf{k}}/\mathrm{d}t)_{\text{scat}}$ depend on the time interval under discussion.[29,28,30] We shall restrict our consideration to times longer than the reciprocal plasma frequency ω^{-1}_{pl}, which is approximately equal to the time required for the buildup of the screening. In this case, one can use the instantaneous quasi-static plasmon-pole approximation for screened Coulomb potential $V^s(q)$[31–33,23]:

$$V^s(q) = V(q)\left[1+\frac{\kappa^2}{q^2+C\kappa^2\left(\dfrac{\hbar q^2}{4m_r\omega_{\text{pl}}}\right)^2}\right]^{-1}, \tag{10}$$

where

$$\kappa^2 = \frac{4\pi(e^2/\epsilon_0)}{\hbar^2\pi^2}\left(m_e\int_0^\infty \mathrm{d}kF^e_{\mathbf{k}} + m_h\int_0^\infty \mathrm{d}kF^h_{\mathbf{k}}\right), \tag{11}$$

$$\omega^2_{\text{pl}} = 4\pi e^2 n_e/(m_r\epsilon_0), \tag{12}$$

$$n_c = 2L^{-3}\sum_{\mathbf{k}} F^c_{\mathbf{k}}. \tag{13}$$

It is noteworthy that charge neutrality $n_e(t)=n_h(t)\equiv n(t)$ holds owing to pair excitation (deexcitation) by light. Here, the carrier density n_c, the screening wavenumber κ (see Ref. 34), and the plasma frequency, ω_{pl}, depend on time, and $C=4$.

For example, for GaAs ($m_r=0.0527m_0$; m_0 is the electron mass in a vacuum), the reciprocal plasma frequency ω^{-1}_{pl} ranges from 40 to 13 fs when the carrier density n ranges from 10^{17} to 10^{18} cm^{-3}. The greater the density, the smaller the corresponding time, since ω_{pl} depends on the carrier density. Since $n>10^{18}$ cm^{-3} during the main part of the exciting pulse in our calculations (see Section 5), our consideration is undoubtedly correct for $t>40$ fs. It stands to reason that the corresponding time increases for smaller densities. However, in the last case, the characteristic times of the carrier–carrier relaxations and the buildup of the screening become larger than the exciting pulse duration $t_p\sim 100$ fs. Therefore, for small densities, the influence of the processes under discussion on the carrier kinetics is of minor importance.

For times longer than the reciprocal plasma frequency ω^{-1}_{pl}, the scattering terms $(\mathrm{d}P_{\mathbf{k}}/\mathrm{d}t)_{\text{scat}}$ and $(\mathrm{d}F^c_{\mathbf{k}}/\mathrm{d}t)_{\text{scat}}$ can be described in the framework of the Boltzmann equation[35,21,36,37] [see Eqs. (A1) of Appendix A].

A full kinetic treatment with scattering terms determined by the Boltzmann equation is numerically too demanding. Therefore we employ an approximation that correctly describes the scattering terms' behavior with density and temperature. In the case that distribution functions $F_{\mathbf{k}}^c$ are different from quasi-equilibrium Fermi distributions $f_{\mathbf{k}}^c[\mu_c(t),T(t)]$, but not by much, one can linearize the scattering terms $(\mathrm{d}P_{\mathbf{k}}/\mathrm{d}t)_{\mathrm{scat}}$ and $(\mathrm{d}F_{\mathbf{k}}^c/\mathrm{d}t)_{\mathrm{scat}}$ with respect to the deviation $\delta F_{\mathbf{k}}^c \equiv F_{\mathbf{k}}^c - f_{\mathbf{k}}^c[\mu_c(t),T(t)]$. In particular, the linearization is favored by the high densities and, consequently, the high scattering rates. The quasi-equilibrium Fermi distributions $f_{\mathbf{k}}^c[\mu_c(t),T(t)]$ are determined by both the time-dependent chemical potentials $\mu_c(t)$ and the carriers' temperature $T(t)$.[21,27,23]

As to carrier–phonon scattering terms, we consider the phonon system (of LO phonons) to be maintained at a constant temperature T_0 during ultrafast laser excitation owing to its large heat capacity. Substitution of (quasi)equilibrium distribution functions for carriers and LO phonons, whose temperatures are *different,* into the right-hand side of Eq. (A1) of Appendix A, results in the term $(\mathrm{d}F_{\mathbf{k}}^c/\mathrm{d}t)_{\mathrm{c\text{-}ph}}^{(0)}$, which describes the energy transfer between carriers and the LO phonon system (see Appendix B). Superscript 0 means that $(\mathrm{d}F_{\mathbf{k}}^c/\mathrm{d}t)_{\mathrm{c\text{-}ph}}^{(0)}$ is the zero-order term with respect to $\delta F_{\mathbf{k}}^c$.

The rigorously linearized scattering terms $\sim\delta F_{\mathbf{k}}^c$ also contain nondiagonal terms in $\mathbf{k}$.[21,30,38] Neglecting the nondiagonal terms results in a relaxation-time approximation[21,35,38]

$$\left(\frac{\mathrm{d}F_{\mathbf{k}}^c}{\mathrm{d}t}\right)_{\mathrm{scat}} = \left(\frac{\mathrm{d}F_{\mathbf{k}}^c}{\mathrm{d}t}\right)_{\mathrm{c-ph}}^{(0)} - \langle\Gamma_{\mathbf{k}}^c\rangle\{F_{\mathbf{k}}^c - f_{\mathbf{k}}^c[\mu_c(t),T(t)]\}, \tag{14}$$

$$\left(\frac{\mathrm{d}P_{\mathbf{k}}}{\mathrm{d}t}\right)_{\mathrm{scat}} = -\langle\gamma_{\mathbf{k}}\rangle P_{\mathbf{k}}, \tag{15}$$

where $\langle\Gamma_{\mathbf{k}}^{e,h}\rangle$ and

$$\langle\gamma_{\mathbf{k}}\rangle = (\langle\Gamma_{\mathbf{k}}^e\rangle + \langle\Gamma_{\mathbf{k}}^h\rangle)/2 \tag{16}$$

are the relaxation rates related to relaxation of the carriers' distribution functions and polarization, respectively. As a consequence of carrier conservation, parameters $\Gamma_{\mathbf{k}}^{e,h}$ have to be $\mathbf{k}$ independent.[21] Therefore we shall use relaxation rates averaged over quasi-equilibrium distributions (the notation $\langle\cdots\rangle$). The quantities $\langle\Gamma_{\mathbf{k}}^c\rangle$ are equal to

$$\langle\Gamma_{\mathbf{k}}^{\mathrm{e}}\rangle = \langle\Gamma_{\mathbf{k}}^{\mathrm{e-e}}\rangle + \langle\Gamma_{\mathbf{k}}^{\mathrm{e-h}}\rangle + \langle\Gamma_{\mathbf{k}}^{\mathrm{e-ph}}\rangle,$$

$$\langle\Gamma_{\mathbf{k}}^{\mathrm{h}}\rangle = \langle\Gamma_{\mathbf{k}}^{\mathrm{h\text{-}h}}\rangle + \langle\Gamma_{\mathbf{k}}^{\mathrm{h\text{-}e}}\rangle + \langle\Gamma_{\mathbf{k}}^{\mathrm{h\text{-}ph}}\rangle, \tag{17}$$

where e–e, h–h, e–h, and c–ph correspond to the electron–electron, hole–hole, electron–hole, and carrier–phonon scattering, respectively. Calculation of scattering terms $(\mathrm{d}F_{\mathbf{k}}^c/\mathrm{d}t)_{\mathrm{c\text{-}ph}}^{(0)}$, $\langle\Gamma_{\mathbf{k}}^{\mathrm{c-c}}\rangle$, $\langle\Gamma_{\mathbf{k}}^{\mathrm{e-h}}\rangle$, and $\langle\Gamma_{\mathbf{k}}^{\mathrm{e-ph}}\rangle$ is carried out in Appendices A and B.

3. NUMERICAL SOLUTION OF COUPLED DIFFERENTIAL EQUATIONS

We solve the coupled equations [Eqs.(3) and (4)]for the initial values of the carriers' density $n_e = n_h = 0$, temperature $T = T_0 = 300\ ^\circ K$, and polarization $P_{\mathbf{k}} = 0$. The scattering terms $(\mathrm{d}P_{\mathbf{k}}/\mathrm{d}t)_{\mathrm{scat}}$ and $(\mathrm{d}F_{\mathbf{k}}^c/\mathrm{d}t)_{\mathrm{scat}}$ are determined by Eqs. (14)–(17).

We used Eqs. (8) and (10)–(13) for the calculation of the generalized Rabi frequency, $U_{\mathbf{k}}$, Eqs. (6), (7), and (5) for the calculation of $\Delta_{\mathbf{k}}(t)$, and Eqs. (11), (B4), and (B5) for the calculation of carrier–phonon scattering term $(\mathrm{d}F_{\mathbf{k}}^c/\mathrm{d}t)_{\mathrm{c\text{-}ph}}^{(0)}$. Relaxation rates $\langle\Gamma_{\mathbf{k}}^c\rangle$ and $\langle\gamma_{\mathbf{k}}\rangle$ are defined by the quantities $\langle\Gamma_{\mathbf{k}}^{\mathrm{c-c}}\rangle$, $\langle\Gamma_{\mathbf{k}}^{\mathrm{e-h}}\rangle$, and $\langle\Gamma_{\mathbf{k}}^{\mathrm{c-ph}}\rangle$. The last are determined by the corresponding equations in Appendices A and B.

We integrated Eqs. (3) and (4) by the Runge–Kutta method. We calculated quasi-equilibrium Fermi distributions, $f_{\mathbf{k}}^c[\mu_c(t),T(t)]$, by nonequilibrium distribution functions of electrons, $F_{\mathbf{k}}^e$ and holes, $F_{\mathbf{k}}^h$, found at the previous time step, using Eq. (13) for the carrier density $n(t)$ and the formula for the total kinetic-energy density

$$\langle\epsilon_{\mathrm{kin}}\rangle = 2L^{-3}\sum_{\mathbf{k},c}\epsilon_k^{0c}F_{\mathbf{k}}^c. \tag{18}$$

As a first step, we evaluated the carriers' temperature $T(t)$ by Eqs. (B10) and (B13) of Ref. 21, linking $\langle\epsilon_{\mathrm{kin}}\rangle$ and temperature. Then, using $n(t)$ and $T(t)$, we calculated the chemical potentials, μ_c, from Eq. (B9) of Ref. 21

4. APPROXIMATE MODELS

The solutions corresponding to Eqs. (3), (4), and (6)–(8) are termed "the total model" for short, bearing in mind that they take into account the relaxations related to carrier–carrier and to carrier–phonon scatterings, and the many-body effects: the bandgap renormalization [see Eqs. (6) and (7)] and Coulomb electron–hole correlations [the second term on the right-hand side of Eq. (8)]. In this section we describe a number of approaches to the total model.

A. Free-Carrier Model

For pulses much shorter than the characteristic relaxation times of the system, one can ignore the scattering terms $(\mathrm{d}F_{\mathbf{k}}^c/\mathrm{d}t)_{\mathrm{scat}}$ and $(\mathrm{d}P_{\mathbf{k}}/\mathrm{d}t)_{\mathrm{scat}}$ on the right-hand side of Eqs. (3) and (4). If, in addition, one neglects the bandgap renormalization ($\Delta\epsilon_{\mathbf{k}} = 0$) and Coulomb electron–hole correlations [$U_{\mathbf{k}} = d_{\mathrm{cv}}\mathcal{E}(t)/\hbar$], one arrives at the free-carrier model. In this case, our system can be described as an ensemble of independent two-level systems with different transition frequencies corresponding to a pure inhomogeneously broadened interband transition. In this situation, Eqs. (3) and (4) can be integrated independently for each $\mathbf{k}$. Solutions of the resulting undamped equations are interesting from the point of view of increasing the possible number of carriers due to coherent effects, as these solutions ignore all the irreversible relaxations that destroy coherence.

An analytic solution of the resulting undamped equations for a chirped pulse of special shape exists[39,40] (see

Appendix C). The corresponding solution for $n(\infty)$ [see Eq. (C2) of Appendix C] is symmetric with respect to the sign of the chirp.

B. Solely Relaxation Model

If one neglects the bandgap renormalization and Coulomb electron-hole correlations ($\Delta\epsilon_{\mathbf{k}}=0$ and $U_{\mathbf{k}}=d_{cv}\mathcal{E}(t)/\hbar$) in the total model, one arrives at the solely relaxation model. Comparisons between the solely relaxation model behavior and those of the free-carrier and total models will enable us to study the influence of the relaxation and many-body effects, respectively, on the chirped-pulse control of carriers.

C. Partial Many Body Effects Model

The many-body effects include both the bandgap renormalization (diagonal effect) and Coulomb electron–hole correlations. If one neglects these correlations in the total model [$U_{\mathbf{k}}=d_{\mathrm{cv}}\mathcal{E}(t)/\hbar$], one arrives at the partial many-body effects model, including only the bandgap renormalization. It should be emphasized that the partial many-body effects model does take into account the relaxation effects described by scattering terms $(\mathrm{d}F^{e}_{\mathbf{k}}/\mathrm{d}t)_{\mathrm{scat}}$ and $(\mathrm{d}P_{\mathbf{k}}/\mathrm{d}t)_{\mathrm{scat}}$. Therefore comparisons between the last model behavior and that of the total model will enable us to study separately the influence of the bandgap renormalization and Coulomb electron–hole correlations on the chirped-pulse control of carriers.

5. RESULTS AND DISCUSSION

We consider linear chirped pulses of the form

$$\mathcal{E}(t)\exp[i\varphi(t)]=\mathcal{E}_0\exp\left[-\frac{1}{2}(\delta^2-i\mu)(t-t_0)^2\right]. \quad (19)$$

If chirped pulses are obtained by changing the separation of pulse-compression gratings, the parameters δ and μ are determined by the formulas[16,13]

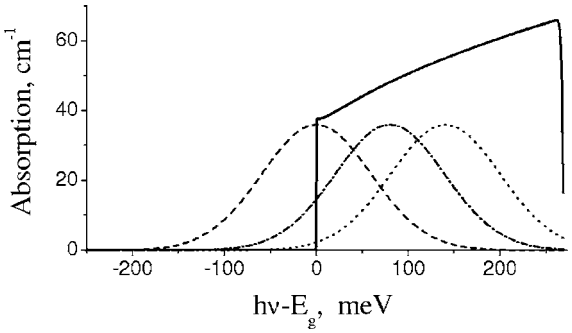

Fig. 2. Continuum part of the bandgap absorption spectrum in an unexcited sample (solid curve), calculated by the Elliott formula,[23,27], together with exciting pulse spectra for different detunings of the carrier pulse frequency, ω, with respect to the semiconductor optical gap $\hbar\Delta_0=\hbar\omega-E_g=0$ (dashed curve), 80 (dashed–dotted curve) and 140.4 (dotted curve) meV. The Elliott formula is adjusted for the dipole moment dependence on the carrier energy [Eq. (9)].

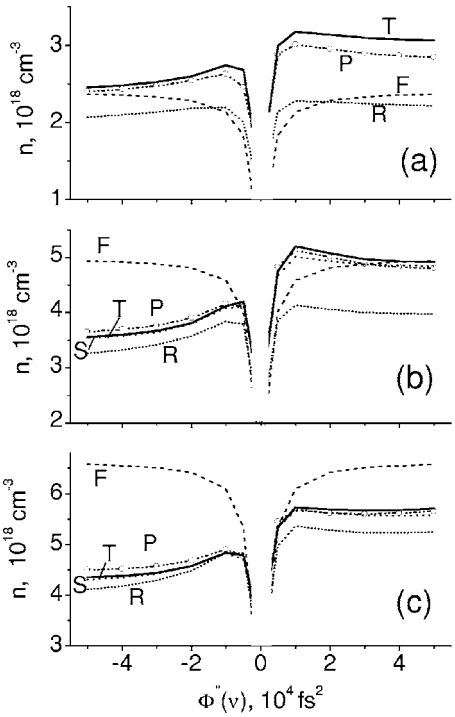

Fig. 3. Excited carrier densities n after the completion of the pulse action as functions of $\Phi''(\nu)$ for different detunings (a) $\hbar\Delta_0=0$, (b) 80, and (c) 140.4 meV. T, total model; F, free-carrier model; R, solely relaxation model; S, simplified relaxation model[24] $\langle\Gamma^{e}_{\mathbf{k}}\rangle=\langle\Gamma^{h}_{\mathbf{k}}\rangle=17\ \mathrm{ps}^{-1}$ adjusted for many-body effects (see text); P, partial many-body effects model.

$$\delta^2=\{\tau_0^2+[\Phi''^2(\omega)/\tau_0^2]\}^{-1},\quad \mu=-\Phi''(\omega)[\tau_0^4+\Phi''^2(\omega)]^{-1}, \quad (20)$$

where $\tau_0=t_{p0}/(2\sqrt{\ln 2})$, t_{p0} is the pulse duration of the corresponding transform-limited pulse, and $\Phi''(\omega)=\Phi''(\nu)/(4\pi^2)$, $\Phi''(\nu)$ the chirp rate in the frequency domain. In addition to t_{p0}, the transform-limited pulse is characterized by the dimensionless pulse area $S_0=1/\hbar\int_{-\infty}^{\infty}d_{\mathrm{cv}}\mathcal{E}(t)\mathrm{d}t=d_{\mathrm{cv}}\mathcal{E}_0[\Phi''(\omega)=0]\tau_0\sqrt{2\pi}/\hbar$. The pulse chirping does not change a pulse spectrum and its energy; it stretches only a pulse and reduces its peak intensity.

All calculations were performed for an optically thin bulk sample of GaAs at room temperature for $t_{p0}=13$ fs and $S_0=1.5\pi$ and different detunings of the carrier-pulse energy $\hbar\omega$ with respect to the semiconductor optical gap E_g: $\hbar\Delta_0=0$, 80, and 140.4 meV. The continuum part of the bandgap-absorption spectrum in such a sample when it is unexcited is shown in Fig. 2 along with exciting pulse spectra for the detunings listed. It is noteworthy that the used pulse parameters correspond to moderately strong fields. For example, $\mathcal{E}_0\simeq 15\times10^5$ V/cm for $|\Phi''(\nu)|=10^4$ fs^2. The values of the GaAs parameters were taken from Refs. [21,22] (m_0 is the electron mass in vacuum):

m_e	effective electron mass	$0.067m_0$
m_h	effective hole mass	$0.247m_0$
E_g	bandgap	1.519 eV
d_{cv}	transition dipole moment	25.0×10^{-18} CGSE

ϵ_0	static electric constant	12.3
$\hbar\omega_0$	LO phonon energy	36 meV
α	Fröhlich constant	0.069

Figure 3 shows the excited carrier density after the completion of the pulse action as a function of $\Phi''(\nu)$. The calculated dependences $n[\Phi''(\nu)]$ are confined to the values of an argument $|\Phi''(\nu)|>5000$ fs^2, since our consideration is correct for times larger than the reciprocal plasma frequency. One can see that with a rise in the absolute value of $\Phi''(\nu)$ in the limit of $|\Phi''(\nu)|<10^4$ fs^2, the carrier density n increases for all the models and detunings. For larger values of $|\Phi''(\nu)|>10^4$ fs^2, one can observe smooth variations of n.

Curves F for the free-carrier model are symmetrical with respect to the chirp sign. For other models, n depends on the chirp sign (curves T, R, and P). Figure 3 shows that the larger the frequency detuning Δ_0 is, the larger the asymmetry of carrier-density dependence on the chirp sign is. The carriers' densities n are larger for positive $\Phi''(\nu)$ than those for negative $\Phi''(\nu)$ of the same absolute value $|\Phi''(\nu)|$.

Including relaxation in the solely relaxation model (curves R) results in diminishing n relative to the free-carrier model (curves F). This diminishing depends on the frequency detuning Δ_0. The larger the frequency detuning Δ_0 is, the larger the influence of relaxation on the excited carriers' density is. This last effect also depends on the chirp sign and therefore contributes to the asymmetry in the corresponding curves.

Including many-body effects in the total (curves T) and partial many-body effects (curves P) model enlarges the excited carrier densities in comparison with the solely relaxation model (curves R). This increase is largest for small detunings ($\Delta_0=0$, near the band edge) [Fig. 3(a)] and diminishes when the excitation frequency is well above the bandgap ($\hbar\Delta_0=140.4$ meV) [Fig. 3(c)]. It results in the largest values of n, which correspond to the total model when $\Delta_0=0$, and the free-carrier model when $\hbar\Delta_0=140.4$ meV. In addition, the many-body effects contribute to the asymmetry of the carrier densities' dependence on the chirp sign. The densities are larger for positive chirp.

Furthermore, curves P are very close to the corresponding curves T when the carrier frequency is above the band gap [Figs. 3(b) and 3(c)]. Curves T are slightly higher than corresponding curves P for small detunings ($\Delta_0=0$, near the band edge) [Fig. 3(a)], which can be explained by Coulomb enhancement.[27] As a matter of fact, Coulomb electron–hole correlations are of secondary importance in the case under consideration. It means that the partial many-body effects model would suffice to describe our simulation results.

A. Adiabatic Criterion in the Free-Carrier Model

To understand the behavior shown in Fig. 3, we shall first discuss the free-carrier model. This is an ensemble of independent two-level systems with different transition frequencies corresponding to a purely inhomogeneous broadened interband transition. We shall consider strongly chirped pulses when the pulse duration is much longer than that of the transform-limited one. Then (see Ref. 41)

$$|\Phi''(\omega)| \gg \tau_0^2. \tag{21}$$

For these conditions, the main adiabatic criterion for a two-level system for resonance interaction[1] is the following:

$$\left|\frac{d\omega(t)}{dt}\right| \ll |U_{\mathbf{k}}(t)|^2. \tag{22}$$

For linear chirped pulses determined by Eqs. (19) and (20), we obtain from Eq. (22)

$$S_0 \gg \sqrt{2\pi}. \tag{23}$$

The value of $S_0=1.5\pi$ used in our calculations exceeds the right-hand side of Eq. (23), but not by much. By this means, increasing n, shown in Fig. 3 for the free-carrier model in the region of $|\Phi''(\nu)|\lesssim 10^4$ fs^2, can be explained by signatures of ARP, bearing in mind a sweeping of the pulse frequency through a resonance for quantum transitions in the excitation region (see Fig. 2). The interplay of ARP with IPDP will be discussed in Section 6.

According to Eq. (23), the main adiabatic criterion for the excitation of the free-carrier model with strongly chirped pulses is determined only by the area of the transform-limited pulse and does not depend on the phase term $\Phi''(\omega)$. The point is that both the chirp rate and the square of the Rabi frequency decrease as $1/|\Phi''(\omega)|$ under the conditions considered [see Eqs. (19)–(21)]. Therefore the fulfillment of inequality (22) is not affected by $\Phi''(\omega)$.

B. Signatures of ARP in the Solely Relaxation, Partial Many-Body Effects, and Total Models

According to Ref. 14, relaxation does not break the adiabaticity of a process for strong interaction when the Rabi frequency exceeds the reciprocal irreversible dephasing time. Although this condition has been obtained for a molecular system, from the physical standpoint it must also be satisfied in our case, i.e.,

$$|U_{\mathbf{k}}(t)| \gg \langle\gamma_{\mathbf{k}}\rangle, \tag{24}$$

For linear strongly chirped pulses determined by Eqs. (19)–(21), we obtain by Eq. (24)

$$S_0\left[\frac{2\pi}{|\Phi''(\nu)|}\right]^{1/2} \gg \langle\gamma_{\mathbf{k}}\rangle. \tag{25}$$

For $S_0=1.5\pi$ and $|\Phi''(\nu)|=10^4$ fs^2, the left-hand side of Eq. (25) is about 1/10 fs^{-1}, more than the value of the relaxation rate for polarization $\langle\gamma_{\mathbf{k}}\rangle$. This means the conservation of the ARP signatures for all the models that take relaxation into account, i.e., the solely relaxation, partial many-body effects and total models, when $|\Phi''(\nu)|\lesssim 10^4$ fs^2. The latter explains the behavior of the dependences $n[\Phi''(\nu)]$ in Fig. 3 for these models, which is similar to that of the free-carrier model in the region $|\Phi''(\nu)|\lesssim 10^4$ fs^2, at least for positive chirps. For larger values of $|\Phi''(\nu)|>10^4$ fs^2, inequality (25) breaks down. Under these conditions, a coherent ARP signature gives way to an incoherent behavior.

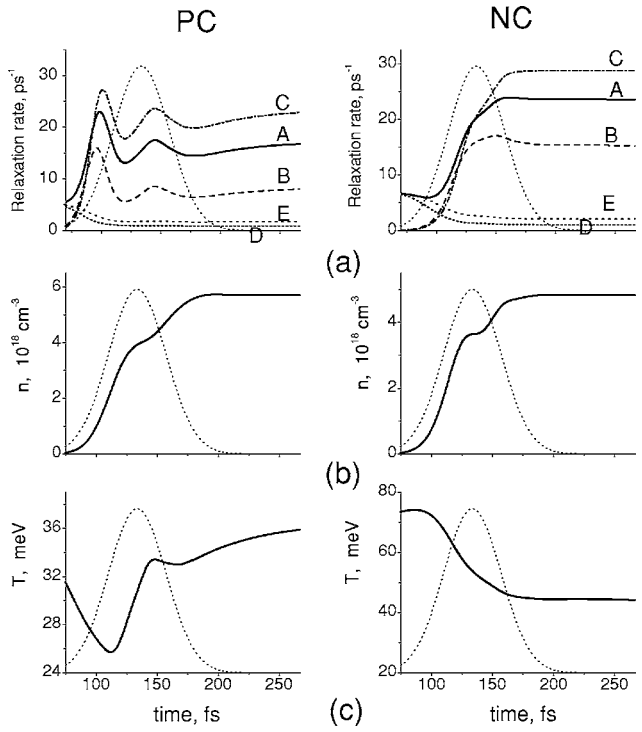

Fig. 4. (a) Relaxation rates [$\langle\gamma_{\mathbf{k}}\rangle$ (A), $\langle\Gamma_{\mathbf{k}}^{e-e}\rangle+\langle\Gamma_{\mathbf{k}}^{e-h}\rangle$ (B), $\langle\Gamma_{\mathbf{k}}^{h-h}\rangle+\langle\Gamma_{\mathbf{k}}^{h-e}\rangle$ (C), $\langle\Gamma_{\mathbf{k}}^{e-ph}\rangle$ (D) and $\langle\Gamma_{\mathbf{k}}^{h-ph}\rangle$ (E)], (b) carrier density, and (c) carrier temperature as functions of time for PC [left column, $\Phi''(\nu)=10^4$ fs^2] and NC [right column, $\Phi''(\nu)=-10^4$ fs^2] excitation. Detuning is $\hbar\Delta_0=140.4$ meV. The exciting pulse shape $[\mathcal{E}(t)/\mathcal{E}_0]^2$ is also shown at each graph (dotted curves).

Since the adiabatic criterion for all the models, taking into account relaxation, depends on $\langle\gamma_{\mathbf{k}}\rangle$ [see Eqs. (24) and (25)], we show in Fig. 4(a) time behaviors of relaxation rates for the total model when chirp rates in the frequency domain are equal to $\Phi''(\nu)=\pm10^4$ fs^2 for PC and NC pulses, respectively. By virtue of the fact that relaxation parameters in our approximation depend on the carrier density n and their temperature T [see Eqs. (A11)–(A14)], we show in Figs. 4(b) and 4(c) $n(t)$ and $T(t)$, respectively, as functions of time as well. One can see that, at the beginning of the exciting pulse, relaxation rates $\langle\gamma_{\mathbf{k}}\rangle$, $\langle\Gamma_{\mathbf{k}}^{e-e}\rangle+\langle\Gamma_{\mathbf{k}}^{e-h}\rangle$, and $\langle\Gamma_{\mathbf{k}}^{h-h}\rangle+\langle\Gamma_{\mathbf{k}}^{h-e}\rangle$ increase over time owing to the increase of the carrier density and then tend toward constant values. The average values of $\langle\gamma_{\mathbf{k}}\rangle$ over the pulse are close to that used previously for the simplified relaxation model[24] when $(dF_{\mathbf{k}}^{c}/dt)_{c-ph}^{(0)}=0$ and $\langle\Gamma_{\mathbf{k}}^{e}\rangle=\langle\Gamma_{\mathbf{k}}^{h}\rangle=\langle\gamma_{\mathbf{k}}\rangle=\text{const}=17$ ps^{-1}. It is noteworthy that the dependence $n[\Phi''(\nu)]$, calculated for the simplified relaxation model[24] adjusted for the many-body effects, is very close to that of the total model (see curves T and S of Figs. 3(b) and 3(c)).

6. TIME EVOLUTION OF NONEQUILIBRIUM DISTRIBUTION FUNCTIONS: TIME-DEPENDENT QUASI-PARTICLE ("DRESSED" ELECTRONS AND HOLES) DISPERSION

We have explained the increasing n, shown in Fig. 3, for the solely relaxation, partial many-body effects, and total models in the region of $|\Phi''(\nu)|\lesssim10^4$ fs^2 via signatures of ARP. In addition, Fig. 3 shows that a PC pulse is more effective for generating electron–hole pairs in these models than a NC pulse. To understand this behavior, we shall consider the second condition to the adiabatic criterion in terms of Ref. 14. To achieve a total population transfer, a transition must start and end far from resonance to avoid IPDP.[15,16] To clarify to what extent the last condition is satisfied for interband transitions in direct semiconductors, we shall consider the time behavior of nonequilibrium distribution functions for PC and NC excitations.

Since, for the isotropic model, $n_c=2L^{-3}\Sigma_{\mathbf{k}}F_{\mathbf{k}}^{c}=(1/\pi^2)\int_0^\infty k^2F_{\mathbf{k}}^{c}dk$, Fig. 5 presents the time evolution of the weighted nonequilibrium distribution functions, $k^2F_{\mathbf{k}}^{e,h}(t)$, calculated by solving coupled differential equations (3) and (4) for the total model when $\Phi''(\nu)=\pm10^4$ fs^2. In addition, Fig. 5 shows renormalized electron energies corresponding to the conduction band

$$\epsilon_{\mathbf{k}}^{\text{cond}}=\frac{\hbar^2k^2}{2m_e}-\sum_{\mathbf{q}}V^{s}(q)F_{\mathbf{k}+\mathbf{q}}^{e} \tag{26}$$

and the photonic replication of the valence band

$$\epsilon_{\mathbf{k}}^{v}=\hbar\omega(t)-(E_g+\Delta\epsilon_{\text{CH}})-\frac{\hbar^2k^2}{2m_h}+\sum_{\mathbf{q}}V^{s}(q)F_{\mathbf{k}+\mathbf{q}}^{h}. \tag{27}$$

An external electromagnetic field gives rise to interaction between states determined by Eqs. (26) and (27) and, as a

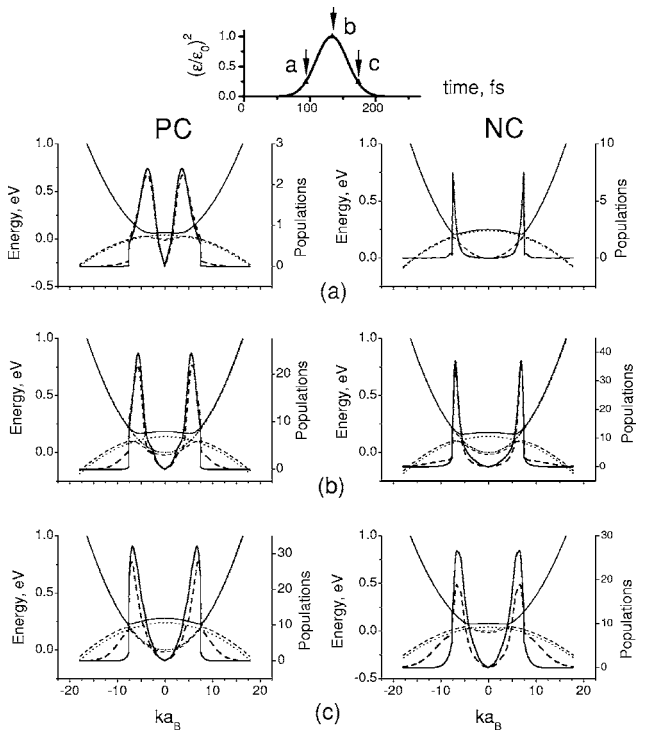

Fig. 5. Energies {left axis; ϵ_k^{cond}, dashed–dotted line; ϵ_k^{v}, dotted curve, dressed states [Eq. (28)] E_1, solid curve and E_2, dashed curve} and the weighted nonequilibrium distribution functions (populations) [right axis; $(ka_B)^2F_{\mathbf{k}}^{e}$, solid curve and $(ka_B)^2F_{\mathbf{k}}^{h}$, dashed curve) as functions of the wave number k at the (a) beginning, (b) middle, and (c) end of the exciting pulse for positive (left column, $\Phi''(\nu)=10^4$ fs^2) and negative (right column, $\Phi''(\nu)=-10^4$ fs^2) chirp. The parameters are identical to those of Fig. 4. Inset, the square of electric field amplitude $[\mathcal{E}(t)/\mathcal{E}_0]^2$ of the exciting pulse in relative units. The arrows show the instants of time corresponding to (a), (b), and (c).

consequence, to the time-dependent dressed states with energies

$$E_{1,2}(t) = \frac{1}{2}\{(\epsilon_{\mathbf{k}}^{\mathrm{cond}} + \epsilon_{\mathbf{k}}^{v}) \mp \hbar[\Delta_{\mathbf{k}}^2(t) + |U_{\mathbf{k}}|^2]^{1/2}\}, \qquad (28)$$

where quantity $\hbar\Delta_{\mathbf{k}}(t) = \epsilon_{\mathbf{k}}^{v} - \epsilon_{\mathbf{k}}^{\mathrm{cond}}$ was determined by Eq. (5). The states, the dispersion of which is described by Eq. (28), are a generalization of the dressed states introduced in Ref. 42 (see also Refs. 43 and 44) to the time-dependent quasi-particles (dressed electrons and holes).

Let us compare the left and right columns of Fig. 5 for PC and NC excitation, respectively. One can see that, at the beginning and the middle of the exciting pulse (Figs. 5(a) and 5(b)), the weighted nonequilibrium distribution functions $k^2F_{\mathbf{k}}^{\mathrm{e,h}}(t)$ are more localized near the avoided crossing for the NC excitation than the PC excitation. This means that the second condition of the adiabatic criterion is better satisfied for PC excitation than for NC excitation. In other words, the signatures of ARP under PC excitation are stronger (IPDP is minimal). This explains the dependence of n on the chirp sign observed in Fig. 3.

Figure 5 shows that the second condition of the adiabatic criterion is not well satisfied for both chirps, since functions $k^2F_{\mathbf{k}}^{\mathrm{e,h}}(t)$ are situated not far from the avoided crossing during the pulse action, and IPDP occurs. The point is that the exciting pulse spectrum is limited and is narrower than the transition bandwidth in our simulations (see Fig. 2). In addition, there are two regions of the avoided crossing in the momentum space that are a limited distance apart. By this means, the population transfer for $|\Phi''(\nu)| \lesssim 10^4$ fs^2, shown in Fig. 3, can be explained by the interplay of ARP with IPDP. However, the signatures of ARP under PC excitation are stronger than those for NC excitation. Correspondingly, the signatures of IPDP under NC excitation are stronger than those for PC excitation.

A. Dependence of Distribution-Function Localization on Chirp Sign

Figure 5 shows that the distribution functions $k^2F_{\mathbf{k}}^{\mathrm{e,h}}(t)$ are more localized near the avoided crossing for NC excitation than those for PC excitation. Such behavior may be attributed to both relaxation and bandgap shrinkage during the excited pulse action.

The relaxation effects are similar to those in molecular systems (see Section 1 and Fig. 1). Consider an excitation with positive detuning $\Delta_0 > 0$ of the carrier pulse frequency ω with respect to the semiconductor optical gap $E_g/\hbar$ (Fig. 2). In the wave-packet picture, the field interaction places amplitudes on the conduction band (Fig. 5). These amplitudes start to slide down the band. Since the wave packets on the conduction band move from higher optical frequencies to lower optical frequencies, they follow the avoided crossing between the conduction band and the photonic replication of the valence band for NC excitation, inducing IPDP, and "run away" from the avoided crossing for PC excitation, suppressing IPDP. This explains the asymmetry of the dependence of n on the chirp sign, observed in Fig. 3, especially for the solely relaxation model (curves R), which increases with the frequency detuning Δ_0.

B. Bandgap Shrinkage Contribution

However, the asymmetry under discussion is larger for the partial many-body effects and total models (curves P and T) than for the solely relaxation model. It means the many-body effects also contribute to the asymmetry. Since the partial many-body effects model would suffice to describe our simulation results (see Section 5), the main contribution arises from the bandgap shrinkage [Eqs. (6) and (7)]. The latter is contained in the quantity $\hbar\Delta_{\mathbf{k}}(t)$ [Eq. (5)], which is the difference between the renormalized electron energies [Eqs. (26) and (27)]:

$$\hbar\Delta_{\mathbf{k}}(t) = \epsilon_{\mathbf{k}}^{v} - \epsilon_{\mathbf{k}}^{\mathrm{cond}} = (\epsilon_{\mathbf{k}}^{0,v} - \epsilon_{\mathbf{k}}^{0,\mathrm{cond}}) - \Delta\epsilon_{\mathbf{k}} = [\hbar\omega(t) - E_g - \epsilon_k^{0\mathrm{h}} - \epsilon_k^{0\mathrm{e}}] - \Delta\epsilon_{\mathbf{k}}, \qquad (29)$$

where $\epsilon_{\mathbf{k}}^{0,\mathrm{cond}} = \epsilon_k^{0\mathrm{e}} = \hbar^2k^2/2m_e$ and $\epsilon_{\mathbf{k}}^{0,v} = \hbar\omega(t) - E_g - \epsilon_k^{0h}$ ($\epsilon_k^{0h} = \hbar^2k^2/2m_h$) are the related nonrenormalized energies corresponding to the free-carrier model. The larger the change of $\hbar\Delta_{\mathbf{k}}$ during the exciting pulse action

$$\hbar[\Delta_{\mathbf{k}}(t_f) - \Delta_{\mathbf{k}}(t_i)] = \hbar[\omega(t_f) - \omega(t_i)] - \Delta\epsilon_{\mathbf{k}}(t_f), \qquad (30)$$

the better the second condition of the adiabatic criterion is obeyed. In this case, the distribution functions $k^2F_{\mathbf{k}}^{\mathrm{e,h}}(t)$ are less localized near the avoided crossing, and the signatures of ARP are stronger. The first term on the right-hand side of Eq. (30) is determined by the spectral bandwidth of the exciting pulse. This term is positive for PC excitation and negative for NC excitation, whereas the second term $-\Delta\epsilon_{\mathbf{k}}(t_f)$ (the bandgap shrinkage) is positive. According to the estimations in Appendix D, the bandgap shrinkage reduces the semiconductor optical gap by $\Delta\epsilon_{\mathbf{k}}(t_f) \simeq -41$ meV during pulse action. This means that the change of $\hbar\Delta_{\mathbf{k}}$ is larger than the pulse bandwidth by 41 meV for PC excitation and smaller than the pulse bandwidth by the same value for NC excitation. The change is equivalent to the corresponding increase in the effective spectral bandwidth of the exciting pulse for PC excitation and to the corresponding decrease for NC excitation. Hence the difference between the values of $\hbar[\Delta_{\mathbf{k}}(t_f) - \Delta_{\mathbf{k}}(t_i)]$ for PC and NC excitations comprises $2|\Delta\epsilon_{\mathbf{k}}(t_f)| \simeq 80$ meV. This value is of the same order of magnitude as the spectral bandwidth of the exciting pulse (140 meV). As a matter of fact, the shrinkage influence on the localization of the distribution functions, $k^2F_{\mathbf{k}}^{\mathrm{e,h}}(t)$, must be essential. It amplifies the asymmetry in the dependence of n on the chirp sign observed in Fig. 3 for the total and partial many-body effects models (curves T and P, respectively) with respect to the solely relaxation model (curves R).

Figure 6 illustrates the above issue, presenting the time evolution of the renormalized electron energies defined by Eqs. (26) and (27)) (solid curves) and the related nonrenormalized energies corresponding to the free-carrier model $\epsilon_{\mathbf{k}}^{0,\mathrm{cond}}$ and $\epsilon_{\mathbf{k}}^{0,\mathrm{v}}$ (dotted curves). The bandgap shrinkage is in accordance with the estimations of Appendix D. The first term on the right-hand side of Eq. (30), $\hbar[\omega(t_f) - \omega(t_i)] = \epsilon_{\mathbf{k}}^{0,\mathrm{v}}(t_f) - \epsilon_{\mathbf{k}}^{0,\mathrm{v}}(t_i)$, can be seen as the energy difference between dotted curves representing nonrenormalized photonic replications of the valence band at the end (C) and the beginning (A) of the exciting pulse. The

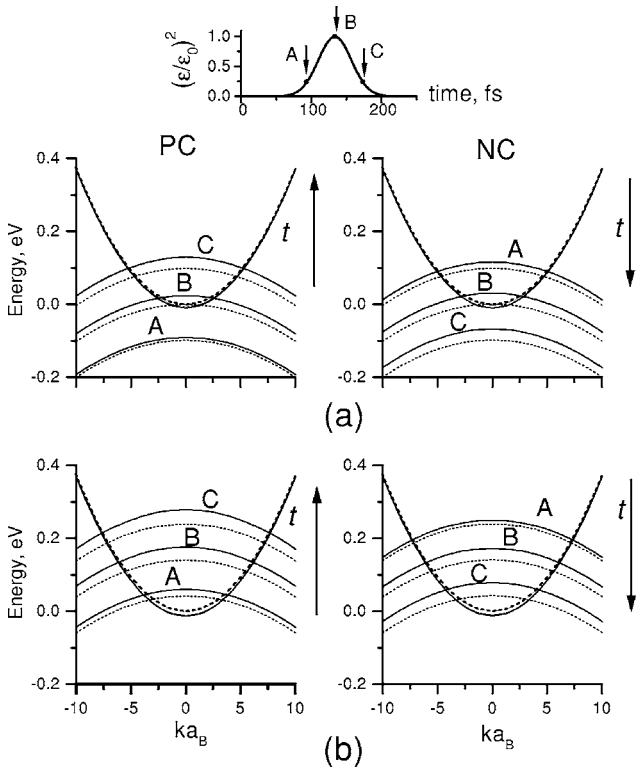

Fig. 6. Time evolution of renormalized electron energies $\epsilon_{\mathbf{k}}^{\mathrm{cond}}$ and $\epsilon_{\mathbf{k}}^{v}$ (solid curves) and the corresponding nonrenormalized energies $\epsilon_{\mathbf{k}}^{0,\mathrm{cond}}$ and $\epsilon_{\mathbf{k}}^{0,v}$ (dotted curves) for positive [left column, $\Phi''(\nu)=10^4$ fs^2] and negative [right column, $\Phi''(\nu)=-10^4$ fs^2] chirp and different detunings (a) $\hbar\Delta_0=0$ and (b) 140.4 meV. The other parameters are identical to those of Fig. 4. Inset, the square of electric field amplitude $[\mathcal{E}(t)/\mathcal{E}_0]^2$ of the exciting pulse in relative units. The arrows show the instants of time corresponding to curves (A), (B), and (C) for the "photonic replications" of the valence band $\epsilon_{\mathbf{k}}^{v}$ and $\epsilon_{\mathbf{k}}^{0,v}$.

total right-hand side of Eq. (30), $\hbar[\Delta_{\mathbf{k}}(t_f)-\Delta_{\mathbf{k}}(t_i)]\simeq[\epsilon_{\mathbf{k}}^{\mathrm{v}}(t_f)-\epsilon_{\mathbf{k}}^{\mathrm{v}}(t_i)]+[\epsilon_{\mathbf{k}}^{0,\mathrm{cond}}-\epsilon_{\mathbf{k}}^{\mathrm{cond}}(t_f)]$, is the energy difference between solid curves representing renormalized photonic replications of the valence band at the end (C) and the beginning (A) of the exciting pulse, plus a small difference between $\epsilon_{\mathbf{k}}^{0,\mathrm{cond}}$ and the lowest solid curve representing a renormalized conduction band at the end of the pulse. One can easily see that the vertical distances between renormalized photonic replications of the valence band, $\epsilon_{\mathbf{k}}^{\mathrm{v}}$, at the beginning (A) and the end (C) of the pulse increase for PC excitation (left column) and decrease for NC excitation (right column) in comparison with those for nonrenormalized photonic replications $\epsilon_{\mathbf{k}}^{0,\mathrm{v}}$. As indicated above, it is equivalent to an increase in effective spectral bandwidth of the exciting pulse for PC excitation, and the corresponding decrease for NC excitation.

As seen in Fig. 3, including the bandgap shrinkage enlarges the excited carrier densities, n, in comparison with the solely relaxation model. Fig. 6 enables us to explain this issue as well. The point is that the renormalized energies intersect at larger $\mathbf{k}$ than those of nonrenormalized ones at the same instants of time (see Fig. 6). Since the density of states is proportional to k^2, the strength of a dipole transition between the renormalized states is larger than that of nonrenormalized states which results in increasing n. Considering the instantaneous intersection points for the pulse maximum (curves B), one can see that this effect is relatively large for small detuning ($\Delta_0=0$) near the band edge (see Fig. 6(a)) and diminishes when the excitation frequency is well above the bandgap ($\hbar\Delta_0=140.4$ meV) (Fig. 6(b)). It explains the largest enhancement of n due to many-body effects at small detuning ($\Delta_0=0$), observed in Fig. 3(a), and the lesser enhancement when $\hbar\Delta_0=140.4$ meV (Fig. 3(b)).

7. CONCLUSION

In this work we studied the possibility of realizing ARP, excited with an intense short chirped pulse (a concept well known in molecular systems), in a bulk direct-gap semiconductor. An ultrafast laser pulse—semiconductor interaction was described by semiconductor Bloch equations. These are essentially time-dependent Hartree–Fock approximations, improved to account for quasi-static screening, which is appropriate for the pulse intensities and carrier densities we reached. The solutions corresponding to these equations were termed the *total model* for short, bearing in mind that they took into account both the relaxations related to carrier–carrier and carrier–phonon scatterings, and many-body effects—the bandgap renormalization and Coulomb electron–hole correlations. The relaxation rates in the total model were calculated within the relaxation-time approximation, refined to properly describe the behavior of carrier–carrier scattering with density and temperature.

The analysis shows that, in spite of complications due to band structure, signatures of ARP accompanied by IPDP should be observable in the dependence of the carriers' density n on the chirp rate in the frequency domain $\Phi''(\nu)$. In addition, the carriers' densities depend on the chirp sign; n is larger for positive $\Phi''(\nu)$ than negative $\Phi''(\nu)$ of the same absolute value $|\Phi''(\nu)|$. To understand this behavior, we introduced the time-dependent quasiparticle (dressed electrons and holes) dispersion in the rotating frame. This picture, along with the analysis of the localization of nonequilibrium distribution functions, provides the explanation for the interplay of ARP with IPDP and its dependence on the chirp sign. The distribution functions are more localized near the avoided crossing during NC excitation than those during PC excitation. Therefore ARP is enhanced (and IPDP is suppressed) for PC pulse excitation, and, correspondingly, ARP is suppressed (and IPDP is enhanced) for NC excitation.

To appreciate the physical mechanism for this behavior, a number of approaches to the total model were invoked: the free-carrier model; the solely relaxation model, which neglected many-body effects; and the partial many-body effects model, which included both relaxation and bandgap renormalization, and neglected Coulomb electron-hole correlations. Comparisons among the behaviors of different models enabled us to study the influence of relaxation and many-body effects on the chirped-pulse control of carriers.

First, Coulomb electron–hole correlations are of secondary importance at the carrier densities reached. The main many-body effects are due to the bandgap renormalization (bandgap shrinkage) during the exciting pulse action and are well described by the partial many-body-effects model.

Second, both relaxation and, most notably, the bandgap shrinkage are responsible for the carriers' density dependence on the chirp sign. Relaxation favors the IPDP for NC pulse excitation and discriminates against it when the pulse chirp is positive. As for the bandgap shrinkage, it enlarges an effective spectral bandwidth of the exciting pulse for PC excitation (enhancing ARP and suppressing IPDP) and decreases the spectral bandwidth for NC excitation (suppressing ARP and enhancing IPDP). As a matter of fact, the bandgap shrinkage, which is the main many-body effect, gives the dominant contribution to the asymmetry of the carriers' density dependence on the chirp sign.

Third, inclusion of many-body effects enlarges the carriers' density in comparison with the solely relaxation model. The picture of the time-dependent renormalized dispersion (Fig. 6) offers an explanation of the carriers' density enhancement due to the bandgap shrinkage.

In conclusion, our calculations show that the dependence of carriers' density n on the chirp rate in the frequency domain $\Phi''(\nu)$ is only slightly affected by details of the time behavior of relaxation rates. The dependence $n[\Phi''(\nu)]$ calculated with average values of relaxation rates over the pulse is very close to that of the total model.

APPENDIX A: CARRIER–CARRIER SCATTERING

The scattering terms $(dP_{\mathbf{k}}/dt)_{\text{scat}}$ and $(dF^c_{\mathbf{k}}/dt)_{\text{scat}}$ can be written as

$$\left(\frac{dF^c_{\mathbf{k}}}{dt}\right)_{\text{scat}} = \Gamma^c_{\text{in}}[\mathbf{k},F](1-F^c_{\mathbf{k}}) - \Gamma^c_{\text{out}}[\mathbf{k},F]F^c_{\mathbf{k}},$$

$$\left(\frac{dP_{\mathbf{k}}}{dt}\right)_{\text{scat}} = -P_{\mathbf{k}}\sum_{\mathbf{k}'}\bar{W}^p_{\mathbf{k}'\mathbf{k}} + \sum_{\mathbf{k}'}\bar{W}^p_{\mathbf{k}\mathbf{k}'}P_{\mathbf{k}} \tag{A1}$$

in the framework of the Boltzmann equation.[35,21,36,37] Here, $\Gamma^c_{\text{in}}[\mathbf{k},F]=\Sigma_{\mathbf{k}'}\bar{W}^c_{\mathbf{k}\mathbf{k}'}F^c_{\mathbf{k}'}$, $\Gamma^c_{\text{out}}[\mathbf{k},F]=\Sigma_{\mathbf{k}'}\bar{W}^c_{\mathbf{k}'\mathbf{k}}(1-F^c_{\mathbf{k}'})$, $\bar{W}^c_{\mathbf{k}'\mathbf{k}}$ is the Boltzmann scattering matrix for carriers, and $\bar{W}^p_{\mathbf{k}'\mathbf{k}}$ is the scattering matrix for the polarization. The scattering matrices $\bar{W}^{c,p}_{\mathbf{k}'\mathbf{k}}$ are the sums of the scattering matrices for carrier–carrier and carrier–phonon interactions. In particular,

$$\bar{W}^{\text{e}}_{\mathbf{k}'\mathbf{k}} = \bar{W}^{\text{e-e}}_{\mathbf{k}'\mathbf{k}} + \bar{W}^{\text{e-h}}_{\mathbf{k}'\mathbf{k}} + \bar{W}^{\text{e-ph}}_{\mathbf{k}'\mathbf{k}},$$

$$\bar{W}^{\text{h}}_{\mathbf{k}'\mathbf{k}} = \bar{W}^{\text{h-h}}_{\mathbf{k}'\mathbf{k}} + \bar{W}^{\text{h-e}}_{\mathbf{k}'\mathbf{k}} + \bar{W}^{\text{h-ph}}_{\mathbf{k}'\mathbf{k}}, \tag{A2}$$

where e–e, h–h and e–h correspond to electron–electron, hole–hole and electron–hole scattering, respectively, and c–ph corresponds to carrier–phonon scattering.

A full kinetic treatment with scattering terms determined by Eq. (A1) is numerically too demanding. Therefore we employ the relaxation-time approximation (see Section 2). However, this approximation for carrier–carrier scattering must be used with caution. The point is that outright discarding of nondiagonal terms results in a large overestimation of the relaxation rates at low densities and an incorrect dependence of these rates on density.[45,36,37] The reason is that carrier–carrier scattering processes are strongly peaked in the forward direction at low densities, owing to weak screening. Taking into account contributions with the structure of "in-scattering terms" on the right-hand side of Eqs. (A1), $(\Gamma^c_{\text{in}}[\mathbf{k},F]$ for $(dF^c_{\mathbf{k}}/dt)_{\text{scat}}$, and the second term $\Sigma_{\mathbf{k}'}\bar{W}^p_{\mathbf{k}\mathbf{k}'}P_{\mathbf{k}'}$ for $(dP_{\mathbf{k}}/dt)_{\text{scat}})$, on the other hand, results in physically reasonable values and the density dependence of the relaxation rates.[36] One can take into account the contribution of in-scattering terms in the framework of the relaxation-time approximation by redetermining such diagonal relaxation rates as momentum or energy relaxation.[35] Both relaxation rates are of the same order of magnitude for carrier–carrier scattering and are characterized by a similar density dependence. Below, we use the momentum relaxation rate, which is more convenient for our calculations.

A number of the momentum-relaxation rates for carrier–carrier scattering can be found in the literature.[46,47] For the nondegenerate (ND) case, when the carrier temperature T is much larger than the temperature T_{Fc} (corresponding to the Fermi energy $k_BT_{Fc}=(\hbar^2/2m_c)(3\pi^2n)^{2/3}$), the quantity $\langle\Gamma^{\text{c-c,ND}}_{\mathbf{k}}\rangle$ is given by the formula

$$\langle\Gamma^{\text{c-c,ND}}_{\mathbf{k}}\rangle = \frac{4}{3}\sqrt{\frac{2}{\pi^3}}\frac{E_{Bc}}{\hbar}(T_{Fc}/T)^{3/2}\ln Q_s^{-2}, \tag{A3}$$

where $E_{Bc}=\bar{m}_cE_B$ is the effective Rydberg energy, $E_B=m_re^4/(2\hbar^2\epsilon_0^2)$ the exciton Rydberg energy, $\bar{m}_c\equiv m_c/m_r$ and Q_s the screening wavenumber related to the Debye–Hückel screening $q_s^2=8\pi n(e^2/\epsilon_0)/k_BT$: $Q_s^2=\hbar^2q_s^2/[2m_c(k_BT)]=(16/3\pi)T_{Fc}^{3/2}T_{Rc}^{1/2}/T^2$; $k_BT_{Rc}=E_{Bc}$.

The contribution of the electron–hole scattering to the momentum relaxation rate is[46]

$$\langle\Gamma^{\text{e-h,ND}}_{\mathbf{k}}\rangle = \frac{16}{9\pi^{3/2}}\frac{E_B}{\hbar}(T_n/T)^{3/2}\ln Q_n^{-2}, \tag{A4}$$

where $T\gg T_n=T_{Fc}\bar{m}_c$, $Q_n^2=(16/3\pi)T_n^{3/2}T_R^{1/2}/T^2$, $k_BT_R=E_B$.

Now let us turn our attention to the degenerate (D) case. In this case momentum relaxation rates $\langle\Gamma^{\text{c-c,D}}_{\mathbf{k}}\rangle$ for electron–electron and hole–hole scattering are given by the formula[35,48]

$$\langle\Gamma^{\text{c-c,D}}_{\mathbf{k}}\rangle = \frac{\pi^2}{6}\frac{E_{Bc}}{\hbar}\left(\frac{T}{T_{Fc}}\right)^2\frac{k_F}{\kappa}, \tag{A5}$$

when $T\ll T_{Fc}$. Here, κ is the screening wavenumber given by Eq. (11) and $k_F=(3\pi^2n)^{1/3}$ is the momentum at the Fermi level. Since Eq. (11) for κ is reduced to the Thomas–Fermi formula

$$\kappa^2 = 4\frac{m_r(e^2/\epsilon_0)}{\hbar^2}\left(\frac{3n}{\pi}\right)^{1/3}(\overline{m_e}+\overline{m_h}) \tag{A6}$$

for $T\ll T_{Fc}$, we finally obtain

$$\langle \Gamma_{\mathbf{k}}^{\text{c-c,D}} \rangle = \frac{\pi^{5/2}}{12} \frac{E_{Bc}}{\hbar} \left(\frac{T}{T_{Fc}} \right)^2 \left(\frac{k_B T_{Fc}}{E_{Bc}} \right)^{1/4} \frac{\bar{m}_c^{1/2}}{(\overline{m_e} + \overline{m_h})^{1/2}}. \tag{A7}$$

The momentum relaxation rate due to electron—hole scattering for $T \ll T_n$ was obtained in Ref. 46:

$$\langle \Gamma_{\mathbf{k}}^{\text{e-h,D}} \rangle = \frac{\pi^{5/2}}{12} \frac{E_B}{\hbar} \left(\frac{T}{T_n} \right)^2 \left(\frac{k_B T_n}{E_B} \right)^{1/4} \frac{\bar{m}_e^2 \bar{m}_h^2}{(\overline{m_e} + \overline{m_h})^{1/2}}. \tag{A8}$$

It is noteworthy that factors $(T/T_{Fc})^2$ and $(T/T_n)^2$ in Eqs. (A7) and (A8), respectively, are related to the phase-space restriction in the degenerated case. The factors $(k_B T_{Fc}/E_{Bc})^{1/4}$ and $(k_B T_n/E_B)^{1/4}$ in these equations come from screening.

Equations (A3), (A4), and (A7) correspond to limited cases of ND and D electron–hole plasma, respectively. There are no corresponding analytical expressions in the intermediate region when $T \sim T_{Fc}, T_n$. However, it can be shown from the foregoing equations[46] that relaxation rates are proportional to n for small n:

$$\begin{pmatrix} \langle \Gamma_{\mathbf{k}}^{\text{c-c,ND}} \rangle \\ \langle \Gamma_{\mathbf{k}}^{\text{e-h,ND}} \rangle \end{pmatrix} = \eta g_{\text{ND}} \begin{pmatrix} \bar{m}_c^{-1/2} \\ 2\sqrt{2}/3 \end{pmatrix} n \tag{A9}$$

where $\eta \sim 1$ (see below), and tend to zero as $n^{-7/6}$ when n is very large:

$$\begin{pmatrix} \langle \Gamma_{\mathbf{k}}^{\text{c-c,D}} \rangle \\ \langle \Gamma_{\mathbf{k}}^{\text{e-h,D}} \rangle \end{pmatrix} = g_D \begin{pmatrix} \bar{m}_c^3 \\ \bar{m}_e^2 \bar{m}_h^2 \end{pmatrix} n^{-7/6} \tag{A10}$$

Here

$$g_{ND} = \frac{2\sqrt{\pi} E_B \hbar^2}{(k_B T m_r)^{3/2}} \tag{A11}$$

and

$$g_D = \frac{(\pi/3)^{1/6} E_B^{3/4} (k_B T)^2 m_r^{7/4}}{2^{1/4} 9 \hbar^{9/2} (\overline{m_e} + \overline{m_h})^{1/2}}. \tag{A12}$$

Therefore one can reasonably expect for the relaxation rates under consideration, as a function of n, a smooth curve with a maximum in the intermediate region $T \sim T_{Fc}, T_n$.[46] In the framework of our semiquantitative description for carrier-carrier scattering it will suffice to extend both limiting cases, as a function of n, until the corresponding curves intersect. Flattening of the peak can be achieved by a two-point Pade approximation[49]:

$$\langle \Gamma_{\mathbf{k}}^{c\text{-}c} \rangle = \frac{\eta g_{ND} \bar{m}_c^{-1/2} n}{1 + \eta \dfrac{g_{ND}}{g_D} \bar{m}_c^{-7/2} n^{13/6}}, \tag{A13}$$

$$\langle \Gamma_{\mathbf{k}}^{e\text{-}h} \rangle = \frac{2(\sqrt{2}/3) \eta g_{ND} n}{1 + 2(\sqrt{2}/3) \eta \dfrac{g_{ND}}{g_D} \bar{m}_e^{-2} \bar{m}_h^{-2} n^{13/6}}. \tag{A14}$$

Smoothed dependences, Eqs. (A13) and (A14), are close to the nonsmoothed ones when $\eta = 2$. Such a procedure for $\eta = 2$ is used for calculating the relaxation rates due to carrier-carrier scattering in Sec. 3.

APPENDIX B: CARRIER–PHONON SCATTERING

The relaxation parameters for carrier–phonon scattering $(\mathrm{d}F_{\mathbf{k}}^c/\mathrm{d}t)_{\text{c-ph}}^{(0)}$ and $\langle \Gamma_{\mathbf{k}}^{\text{c-ph}} \rangle$ in Eqs. (14) and (17), respectively, can be calculated, using the scattering matrix $\bar{W}_{\mathbf{k}'\mathbf{k}}^{\text{c-ph}}$ [see Eqs. (A2)], which is given by the Fermi golden rule[35,27]:

$$\bar{W}_{\mathbf{k}'\mathbf{k}}^{(\pm)\text{c-ph}} = \frac{2\pi}{\hbar} |M_{\mathbf{k}'\mathbf{k}}^{\pm\mathbf{q}}|^2 \left[N_{T_0}(\hbar\omega_0) + \frac{1}{2} \pm \frac{1}{2} \right] \delta(\epsilon_k^{0c} - \epsilon_{k'}^{0c} \mp \hbar\omega_0), \tag{B1}$$

where $\bar{W}_{\mathbf{k}'\mathbf{k}}^{(\pm)\text{c-ph}}$ are the rates of carrier–phonon scattering for emission (+) or absorption (−) of LO phonons, $\hbar\omega_0$ is the energy of LO phonons, $N_T(\hbar\omega) = [\exp(\beta\hbar\omega) - 1]^{-1}$ is the Bose function, and $\mathbf{q} = \pm(\mathbf{k} - \mathbf{k}')$ is the transferred momentum. The scattering matrix elements $M_{\mathbf{k}'\mathbf{k}}^{\pm\mathbf{q}}$ are given by the formula

$$|M_{\mathbf{k}'\mathbf{k}}^{\pm\mathbf{q}}|^2 = \delta_{\mathbf{k}', \mathbf{k} \mp \mathbf{q}} \frac{1}{L^3} B(q), \tag{B2}$$

where $\delta_{\mathbf{k}', \mathbf{k} \mp \mathbf{q}}$ is the Kronecker delta and the quantity B is determined by[35]

$$B(q) = \frac{B_0}{q^2} \left(\frac{q^2}{q^2 + \kappa^2} \right)^2 \tag{B3}$$

in the instantaneous quasi-static approximation for screened polar carrier-LO phonon interaction. κ^2 is given by Eq. (11), $B_0 = (1/\tau_{\text{PO}}) \pi \hbar^3 p_0^c / m_c$, $p_0^c = (2 m_c \hbar\omega_0)^{1/2}/\hbar$, $\tau_{\text{PO}} = (2\alpha\omega_0)^{-1}$ is the characteristic time for carrier-LO phonon scattering, $\alpha = e^2 (m_r/2\omega_0)^{1/2} (1/\epsilon_\infty - 1/\epsilon_0)$ and ϵ_∞ is the high-frequency dielectric constant of a semiconductor.

Using Eqs. (B1)–(B3), we obtain for $(\mathrm{d}F_{\mathbf{k}}^c/\mathrm{d}t)_{\text{c-ph}}^{(0)}$:

$$\begin{aligned} \left(\frac{\mathrm{d}F_{\mathbf{k}}^c}{\mathrm{d}t} \right)_{c\text{-}ph}^{(0)} = & -\frac{1}{4} \left(\frac{\hbar\omega_0}{\epsilon_k^{0c}} \right)^{1/2} \frac{1}{\tau_{\text{PO}}} [N_T(\hbar\omega_0) - N_{T_0}(\hbar\omega_0)] \\ & \times \{ [f_F^c(\epsilon_k^{0c} - \hbar\omega_0) - f_F^c(\epsilon_k^{0c})] \, \theta(\epsilon_k^{0c} - \hbar\omega_0) U_c^+ \\ & + [f_F^c(\epsilon_k^{0c} + \hbar\omega_0) - f_F^c(\epsilon_k^{0c})] U_c^- \}, \end{aligned} \tag{B4}$$

where $f_F^c(\epsilon_k^{0c}) \equiv f_{\mathbf{k}}^c[\mu_c(t), T(t)]$, $\theta(\epsilon_k^{0c} - \hbar\omega_0)$ is the Heaviside step function [$\theta(\epsilon_k^{0c} - \hbar\omega_0) = 1$ for $\epsilon_k^{0c} - \hbar\omega_0 > 0$ and $\theta(\epsilon_k^{0c} - \hbar\omega_0) = 0$ for $\epsilon_k^{0c} - \hbar\omega_0 < 0$],

$$\begin{aligned} U_c^{\pm} = & \ln \frac{[(\epsilon_k^{0c} \mp \hbar\omega_0)^{1/2} + (\epsilon_k^{0c})^{1/2}]^2 + \kappa^2 \dfrac{\hbar^2}{2m_c}}{[(\epsilon_k^{0c} \mp \hbar\omega_0)^{1/2} - (\epsilon_k^{0c})^{1/2}]^2 + \kappa^2 \dfrac{\hbar^2}{2m_c}} \\ & + \frac{\kappa^2}{\left(\dfrac{2m_c}{\hbar^2} \right) [(\epsilon_k^{0c} \mp \hbar\omega_0)^{1/2} + (\epsilon_k^{0c})^{1/2}]^2 + \kappa^2} \\ & - \frac{\kappa^2}{\left(\dfrac{2m_c}{\hbar^2} \right) [(\epsilon_k^{0c} \mp \hbar\omega_0)^{1/2} - (\epsilon_k^{0c})^{1/2}]^2 + \kappa^2}. \end{aligned} \tag{B5}$$

Equation (B4) enables us to describe the energy transfer between carriers and the LO phonon system.[35,50] The process under consideration conserves the carriers' densities.

Let us turn to relaxation rates $\langle\Gamma_{\mathbf{k}}^{\text{c-ph}}\rangle$. "The diagonal" in $\mathbf{k}$ relaxation rates before averaging over quasi-equilibrium distributions can be written in the form[35]

$$\Gamma_{\mathbf{k}}^{\text{c-ph}} = \sum_{\mathbf{k}'}\left[\bar{W}_{\mathbf{k}'\mathbf{k}}^{(+)\text{c-ph}}\frac{1-f_F^c(\epsilon_k^{0c}-\hbar\omega_0)}{1-f_F^c(\epsilon_k^{0c})} + \bar{W}_{\mathbf{k}'\mathbf{k}}^{(-)\text{c-ph}}\frac{1-f_F^c(\epsilon_k^{0c}+\hbar\omega_0)}{1-f_F^c(\epsilon_k^{0c})}\right]. \tag{B6}$$

Substituting Eqs. (B1)–(B3) into Eq. (B6), and averaging over quasi-equilibrium distributions, we finally obtain

$$\langle\Gamma_{\mathbf{k}}^{\text{c-ph}}\rangle = \frac{m_c p_0^c}{\hbar^2\pi^2\beta n_c}\frac{1}{\tau_{\text{PO}}}\frac{1}{2}\int_0^\infty\frac{q^3\mathrm{d}q}{(q^2+\kappa^2)^2}([N_{T_0}(\hbar\omega_0)+1] \times\exp(-\beta\hbar\omega_0)\ln\{1+\exp[\beta(\mu_c+\hbar\omega_0-\epsilon_+)]\} + N_{T_0}(\hbar\omega_0)\exp(\beta\hbar\omega_0)\ln\{1+\exp[\beta(\mu_c-\hbar\omega_0 - \epsilon_-)]\}), \tag{B7}$$

where $\epsilon_\pm = \pm\hbar\omega_0/2+(\hbar\omega_0/4)[(q/p_0^c)^2+(p_0^c/q)^2]$, $p_0^c=(2m_c\hbar\omega_0)^{1/2}/\hbar$.

One can see from Eq. (B7) that the carrier–phonon relaxation rate $\langle\Gamma_{\mathbf{k}}^{\text{c-ph}}\rangle$ does not depend on the carrier density for small densities since, in this limit, $\ln\{1+\exp[\beta(\mu_c\pm\hbar\omega_0-\epsilon_\pm)]\}\approx\exp(\beta(\mu_c\pm\hbar\omega_0-\epsilon_\pm))\sim n$.

APPENDIX C: ANALYTICAL SOLUTION

There exist an analytic solution[39,40] of the undamped Bloch equations resulting from Eqs. (3) and (4) for the free-carrier model (no many-body effects) and a chirped pulse of special shape

$$\mathcal{E}(t)=\mathcal{E}_0\,\mathrm{sech}\left(\frac{t-t_0}{\tau}\right),\quad \varphi(t)=\frac{\gamma}{\pi\tau}\int_0^t\tanh\left(\frac{t'-t_0}{\tau}\right)\mathrm{d}t'.$$

After completion of the pulse action and for the initial conditions of Section 3, this solution is the following:

$$F_{\mathbf{k}}^e(\infty)+F_{\mathbf{k}}^h(\infty) = 2\sec[(\gamma+\gamma_0)/2]\sec[(\gamma-\gamma_0)/2] \times\left[\sin^2\left(\frac{\Phi}{2}\right)\cosh^2\left(\frac{\gamma}{2}\right) + \cos^2\left(\frac{\Phi}{2}\right)\sinh^2\left(\frac{\gamma}{2}\right)\right], \tag{C1}$$

where $\Phi=(\sigma^2-\gamma^2)^{1/2}$, $\sigma=(d_{\text{cv}}/\hbar)\int_{-\infty}^{\infty}\mathcal{E}(t')\mathrm{d}t'=(d_{\text{cv}}/\hbar)\mathcal{E}_0\pi\tau$, and $\gamma_0=\pi\tau(\epsilon_k^0/\hbar-\Delta_0)$ are the dimensionless pulse area and detuning, respectively.

Integrating quantity $F_{\mathbf{k}}^e(\infty)+F_{\mathbf{k}}^h(\infty)$ [see Eq. (C1)] with respect to momentum $\mathbf{k}$, and taking into account the limitation on the excitation energy [see Eq. (9)], we obtain

$$n(\infty)=\frac{\sqrt{2}m_r^{3/2}}{\hbar^3\pi^2}\int_0^\infty\mathrm{d}\epsilon\sqrt{\epsilon}\frac{1}{1+\exp[(\epsilon-\epsilon_c)/\hbar\Delta_c]}\frac{\cosh\gamma-\cos\Phi}{\cosh\gamma+\cosh\gamma_0}. \tag{C2}$$

One can see from Eq. (C2) that the solutions for $n(\infty)$ are symmetric with respect to the sign of chirp.

APPENDIX D: EVALUATION OF BANDGAP SHRINKAGE DURING PULSE ACTION

Let us estimate the bandgap shrinkage $\Delta\epsilon_{\mathbf{k}}=\Delta\epsilon_{\text{CH}}+\Delta\epsilon_{\text{SX},\mathbf{k}}$ during the excited-pulse action [see Eqs. (6) and (7)]. Quantities $\Delta\epsilon_{\text{CH}}$ and $\Delta\epsilon_{\text{SX},\mathbf{k}}$ were evaluated in Refs. 23 [Eq. (4.48)] and Ref. 27 [Eq. (9.29)], respectively. Using these equations and introducing the normalized distance r_s between particles via relation[27] $(4\pi/3)r_s^3=1/(na_B^3)$, we obtain

$$\Delta\epsilon_{\text{CH}}=-7.62\frac{E_B r_s^{-1/2}}{(1+8.4r_s^{1/2})^{1/2}}, \tag{D1}$$

$$\Delta\epsilon_{\text{SX},\mathbf{k}}=-0.81E_B r_s^{-1}\left(1-\frac{1}{1+2.51r_s^{-1}}\right), \tag{D2}$$

where $a_B=\hbar^2\epsilon_0/(e^2m_r)$ is the exciton Bohr radius and E_B is the exciton Rydberg energy. In our simulation a typical value of the carrier density after the completion of the pulse action is $n=5\times10^{18}\text{cm}^{-3}$, $E_B=4.2$ meV, and $a_B=14$ nm.[27] Substituting these values into Eqs. (D1) and (D2), we have $\Delta\epsilon_{\mathbf{k}}=\Delta\epsilon_{\text{CH}}+\Delta\epsilon_{\text{SX},\mathbf{k}}\simeq-41$ meV.

ACKNOWLEDGMENTS

We are very grateful to R. Zimmermann for illuminating discussions and useful comments during B. D. F.'s visit to the Humboldt University of Berlin and for reading the manuscript. We thank the participants of a seminar under the direction of T. Elsaesser, particularly M. Woerner and C. Lienau for their comments. This work was supported by the Israel Science Foundation (Grant 41/00-1) and the Ministry of Absorption of Israel.

B. D. Fainberg's e-mail address is fainberg@hait.ac.il.

REFERENCES

1. J. S. Melinger, S. R. Gandhi, A. Hariharan, D. Goswami, and W. S. Warren, "Adiabatic population transfer with frequency-swept laser pulses," J. Chem. Phys. **101**, 6439–6454 (1994).
2. S. Chelkowski, A. Bandrauk, and P. B. Corkum, "Efficient molecular dissociation by a chirped ultrashort infrared laser pulse," Phys. Rev. Lett. **65**, 2355–2358 (1990).
3. B. W. Shore, K. Bergmann, A. Kuhn, S. Schiemann, J. Oreg, and J. H. Eberly, "Laser-induced population transfer in multistate systems: a comparative study," Phys. Rev. A **45**, 5297–5300 (1992).
4. M. Shapiro and P. Brumer, "Coherent and incoherent laser control of photochemical reactions," Int. Rev. Phys. Chem. **13**, 187–230 (1994).
5. R. J. Gordon, and S. A. Rice, "Active control of the dynamics of atoms and molecules," Annu. Rev. Phys. Chem. **48**, 601–641 (1997).
6. N. V. Vitanov, T. Halfmann, B. W. Shore, and K. Bergmann, "Laser-induced population transfer by adiabatic passage

techniques," Annu. Rev. Phys. Chem. **52**, 763–809 (2001).
7. J. Kunde, U. Siegner, S. Arlt, G. Steinmeyer, F. Morier-Genoud, and U. Keller, "Potential of femtosecond chirp control of ultrabroadband semiconductor continuum nonlinearities," J. Opt. Soc. Am. B **16**, 2285–2294 (1999).
8. R. Binder and M. Lindenberg, "Ultrafast adiabatic population transfer in p-doped semiconductor quantum wells," Phys. Rev. Lett. **81**, 1477–1480 (1998).
9. J. M. Fraser and H. M. van Driel, "Quantum interference control of free-carrier density in GaAs," Phys. Rev. B **68**, 085208–085208-14 (2003).
10. M.-O. Mewes, M. R. Andrews, D. M. Kurn, D. S. Durfee, C. G. Townsend, and W. Ketterle, "Output coupler for Bose–Einstein condensed atoms," Phys. Rev. Lett. **78**, 582–585 (1997).
11. L. Allen and J.-H. Eberly, *Optical Resonance and Two-Level Atoms* (Wiley, 1975).
12. E. B. Treacy, "Adiabatic inversion with light pulses," Phys. Lett. A **27**, 421–422 (1968).
13. B. D. Fainberg and V. A. Gorbunov, "Coherent population transfer in molecules coupled with dissipative environment by intense ultrashort chirped pulse," J. Chem. Phys. **117**, 7222–7232 (2002).
14. B. D. Fainberg and V. A. Gorbunov, "Coherent population transfer in molecules coupled with dissipative environment by intense ultrashort chirped pulse. II. A simple model," J. Chem. Phys. **121**, 8748–8754 (2004).
15. S. Ruhman and R. Kosloff, "Application of chirped ultrashort pulses for generating large-amplitude ground state vibrational coherence: a computer simulation," J. Opt. Soc. Am. B **7**, 1748–1952 (1990).
16. G. Cerullo, C. J. Bardeen, Q. Wang, and C. V. Shank, "High-power femtosecond chirped pulse excitation of molecules in solution," Chem. Phys. Lett. **262**, 362–368 (1996).
17. D. J. Tannor and S. A. Rice, "Control of selectivity of chemical reaction via control of wave packet evolution," J. Chem. Phys. **83**, 5013–5018 (1985).
18. G.-R. Unanyan, N. V. Vitanov, and K. Bergmann, "Preparation of entangled states by adiabatic passage," Phys. Rev. Lett. **87**, 137902 (2001).
19. Y. Nagata and K. Yamashita, "Theoretical study on molecular excitation using chirped pulses in the condensed phase," Chem. Phys. Lett. **364**, 144–151 (2002).
20. M. Demirplak and S. A. Rice, "Optical control of molecular dynamics in a liquid," J. Chem. Phys. **116**, 8028–8035 (2002).
21. R. Binder, D. Scott, A. E. Paul, M. Lindberg, K. Henneberger, and S. W. Koch, "Carrier–carrier scattering and optical dephasing in highly excited semiconductors," Phys. Rev. B **45**, 1107–1115 (1992).
22. R. A. Indik, R. Binder, M. Mlejnek, J. V. Moloney, S. Hughes, A. Knorr, and S. W. Koch, "Role of plasma cooling, heating, and memory effects in subpicosecond pulse propagation in semiconductor amplifiers," Phys. Rev. A **53**, 3614–3620 (1996).
23. W. W. Chow, S. W. Koch, and M. Sargent, III, *Semiconductor-Laser Physics* (Springer-Verlag, 1997).
24. B. D. Fainberg, B. Levinsky, and V. A. Gorbunov, "Femtosecond chirped pulse control of photoluminescence and generating electron-hole pairs in broadband semiconductors," J. Lumin. **102–103**, 125–130 (2003).
25. B. M. Garraway and K.-A. Suominen, "Adiabatic passage by light-induced potentials in molecules," Phys. Rev. Lett. **80**, 932–935 (1998).
26. M. Lindberg and S. W. Koch, "Effective Bloch equations for semiconductors," Phys. Rev. B **38**, 3342–3350 (1988).
27. H. Haug and S. W. Koch, *Quantum Theory of the Optical and Electronic Properties of Semiconductors* (World Scientific, 2001).
28. E. Sayed, L. Banyai, and H. Haug, "Coulomb quantum kinetics and optical dephasing on the femtosecond time scale," Phys. Rev. B **50**,1541–1550 (1994).
29. M. Hartmann, H. Stolz, and R. Zimmermann, "Kinetics of screening in optically excited semiconductors," Phys. Status Solidi B **159**, 35–42 (1988).
30. H. Haug and A. P. Jauho, *Quantum Kinetics in Transport and Optics of Semiconductors* (Springer-Verlag, 1996).
31. R. Zimmermann, *Many-Particle Theory of Highly Excited Semiconductors* (Teubner, 1988).
32. H. Haug and S. W. Koch, "Semiconductor laser theory with many-body effects," Phys. Rev. A **39**, 1887–1898 (1989).
33. A. Knorr, R. Binder, M. Lindberg, and S. W. Koch, "Theoretical study of resonant ultrashort-pulse propagation in semiconductors," Phys. Rev. A **46**, 7179–7186 (1992).
34. M. Lindberg, R. Binder, and S. W. Koch, "Theory of the semiconductor photon echo," Phys. Rev. B **45**, 1865–1875 (1992).
35. V. F. Gantmakher and Y. B. Levinson, *Carrier Scattering in Metals and Semiconductors* (North Holland, 1987).
36. S. Haas, F. Rossi, and T. Kuhn, "Generalized Monte Carlo approach for the study of the coherent ultrafast carrier dynamics in photoexcited semiconductors," Phys. Rev. B **53**, 12855–12868 (1996).
37. F. Rossi and T. Kuhn, "Theory of ultrafast phenomena in photoexcited semiconductors," Rev. Mod. Phys. **74**, 895–950 (2002).
38. O. Hess and T. Kuhn, "Maxwell—Bloch equations for spatially inhomogeneous semiconductor lasers. I. Theoretical formulation," Phys. Rev. A **54**, 3347–3359 (1998).
39. Y. N. Demkov and M. Kunike, Vestn. Leningr. Univ. Fiz. Khim. **16**, 39 (1969).
40. F. T. Hioe, "Solution of Bloch equations involving amplitude and frequency modulations," Phys. Rev. A **30**, 2100–2103 (1984).
41. B. D. Fainberg, "Absorption spectrum of intense chirped pulse by molecules in solution and the time evolution of vibrationally nonequilibrium populations," Chem. Phys. Lett. **332**, 181–189 (2000).
42. V. M. Galitskii, S. P. Goreslavskii, and V. F. Elesin, "Electric and magnetic properties of a semiconductor in the field of a strong electromagnetic wave," Sov. Phys. JETP **30**, 117–122 (1970).
43. S. Schmitt-Rink, D. S. Chemla, and H. Haug, "Nonequilibrium theory of the optical Stark effect and spectral hole burning in semiconductors," Phys. Rev. B **37**, 941–955 (1988).
44. K. Henneberg and H. Haug, "Nonlinear optics and transport in laser-excited semiconductors," Phys. Rev. B **38**, 9759–9770 (1988).
45. D. W. Snoke, "Density dependence of electron scattering at low density," Phys. Rev. B **50**, 11583–11591 (1994).
46. M. Combescot and R. Combescot, "Conductivity relaxation time due to electron-hole collision in optically excited semiconductors," Phys. Rev. B **35**, 7986–7991 (1987).
47. N. S. Wingreen and M. Combescot, "Electron–electron scattering: collision integral and relaxation rate," Phys. Rev. B **40**, 3191–3196 (1989).
48. V. A. Gasparov and R. Huguenin, "Electron–phonon, electron–electron and electron–surface scattering in metals from ballistic effects," Adv. Phys. **42**, 393–521 (1993).
49. G. A. Baker, Jr. and P. Graves-Morris, *Padé Approximants* (Addison-Wesley, 1981).
50. S. M. Kogan, "On the theory of hot electrons in semiconductors," Sov. Phys. Solid State **4**, 1813–1819 (1963).